Supplement of Eur. J. Mineral., 34, 573–590, 2022
https://doi.org/10.5194/ejm-34-573-2022-supplement

European Journal of Mineralogy
Open Access

Supplement of

Non-destructive determination of the biotite crystal chemistry using Raman spectroscopy: how far we can go?

Stylianos Aspiotis et al.

Correspondence to: Stylianos Aspiotis (stylianos.aspiotis@uni-hamburg.de)

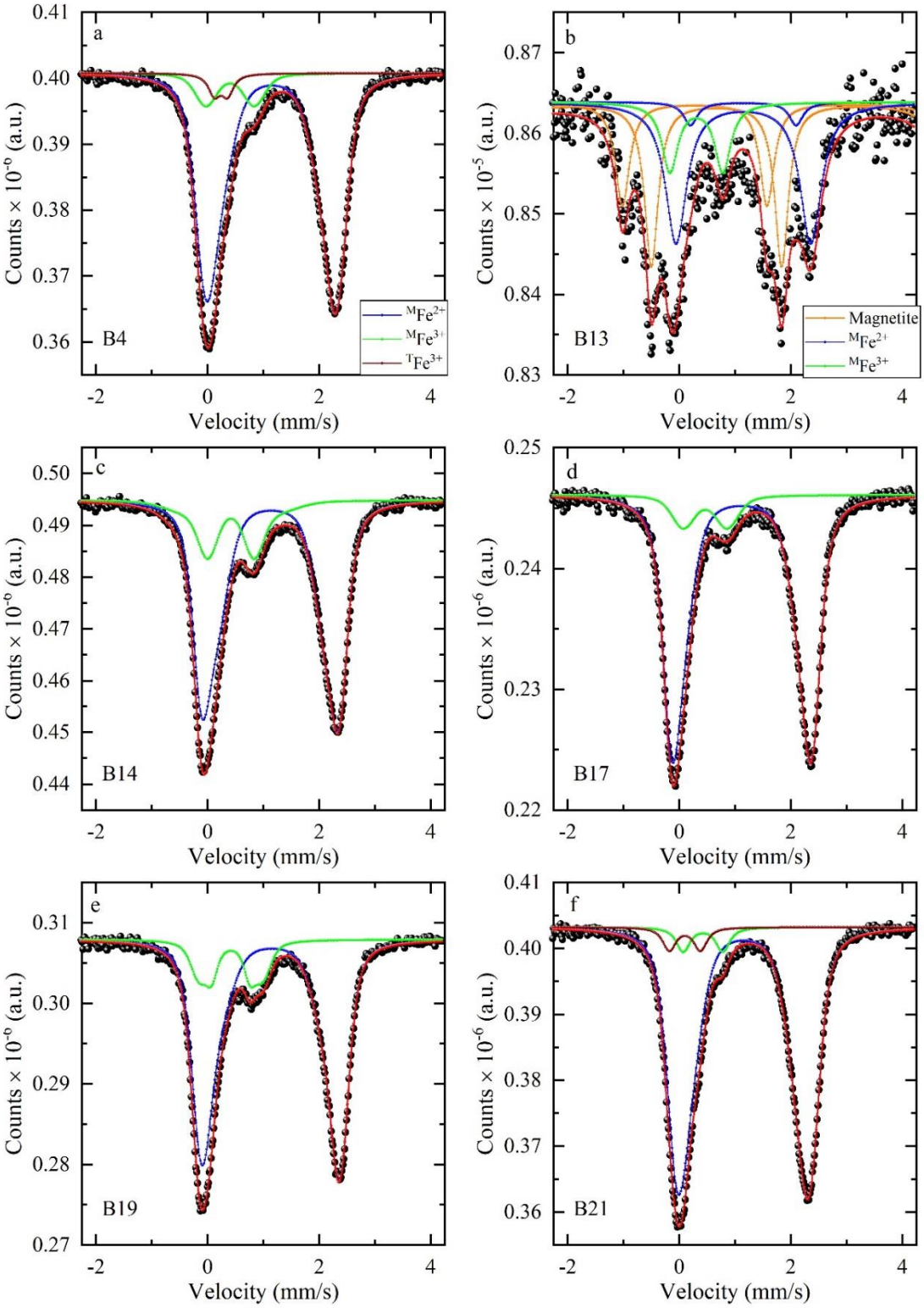

Figure S1: (a) - (f) Room-temperature experimental ^{57}Fe Mössbauer spectra (circles) along with the fitting doublet functions (green, blue, and brown lines) and the resulting spectrum (red line). For sample B13 (b) a classical approach with Lorentzian-shaped doublets (one for $^{M}Fe^{3+}$ and two for $^{M}Fe^{2+}$) was used instead of the quadrupole splitting distribution (QSD) approach due to the presence of magnetite of ~ 70%. For sample B19 (e) the green line is the QSD approach of $^{M}Fe^{3+}$, composed of two doublets due to differences in the local distortion geometry around $^{M}Fe^{3+}$.

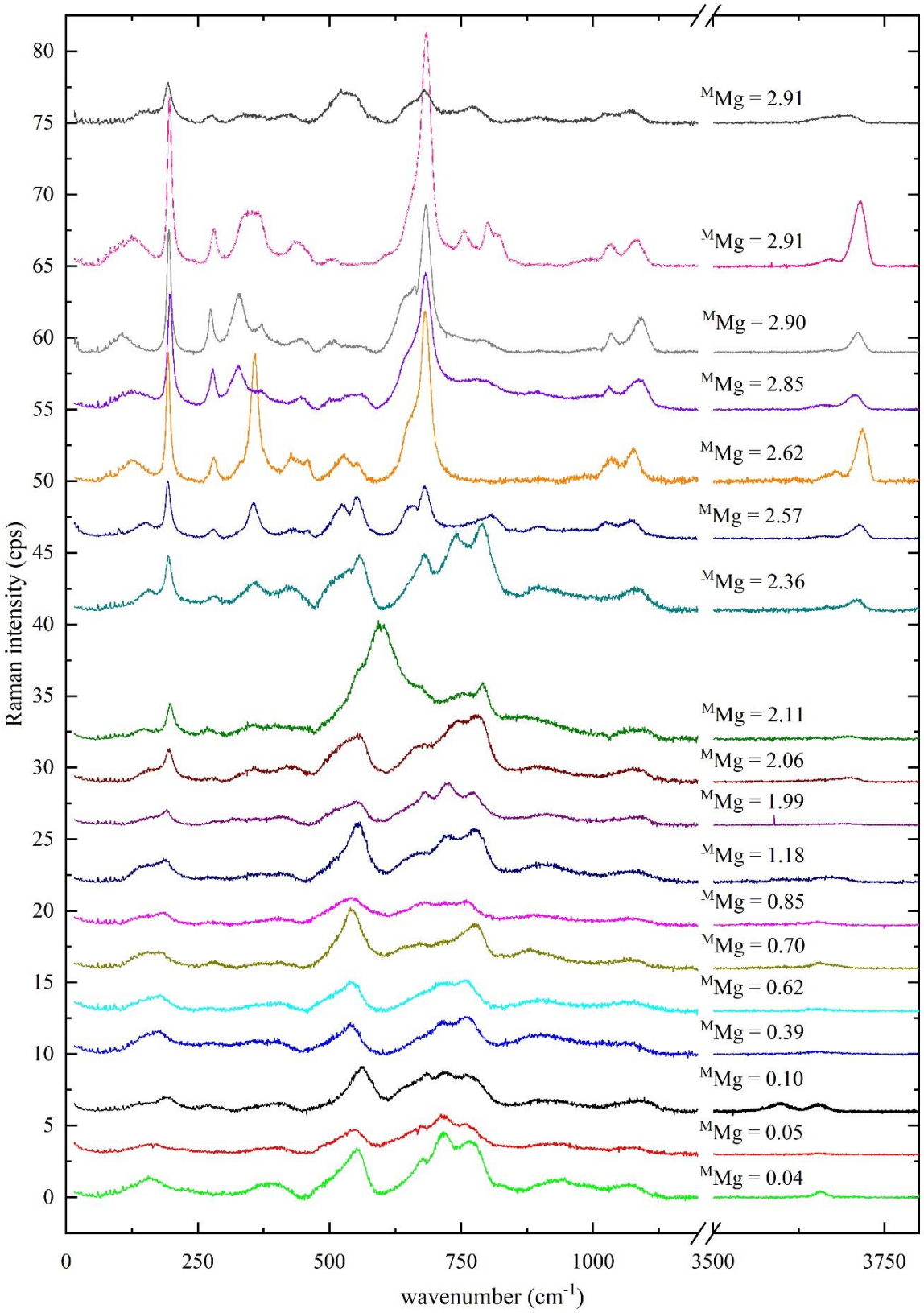

Figure S2: Raman spectra of the analysed biotites in horizontal parallel-polarized geometry, where ^{M}Mg content in apfu increases from bottom to top. For better comparison, the spectra are vertically offset.

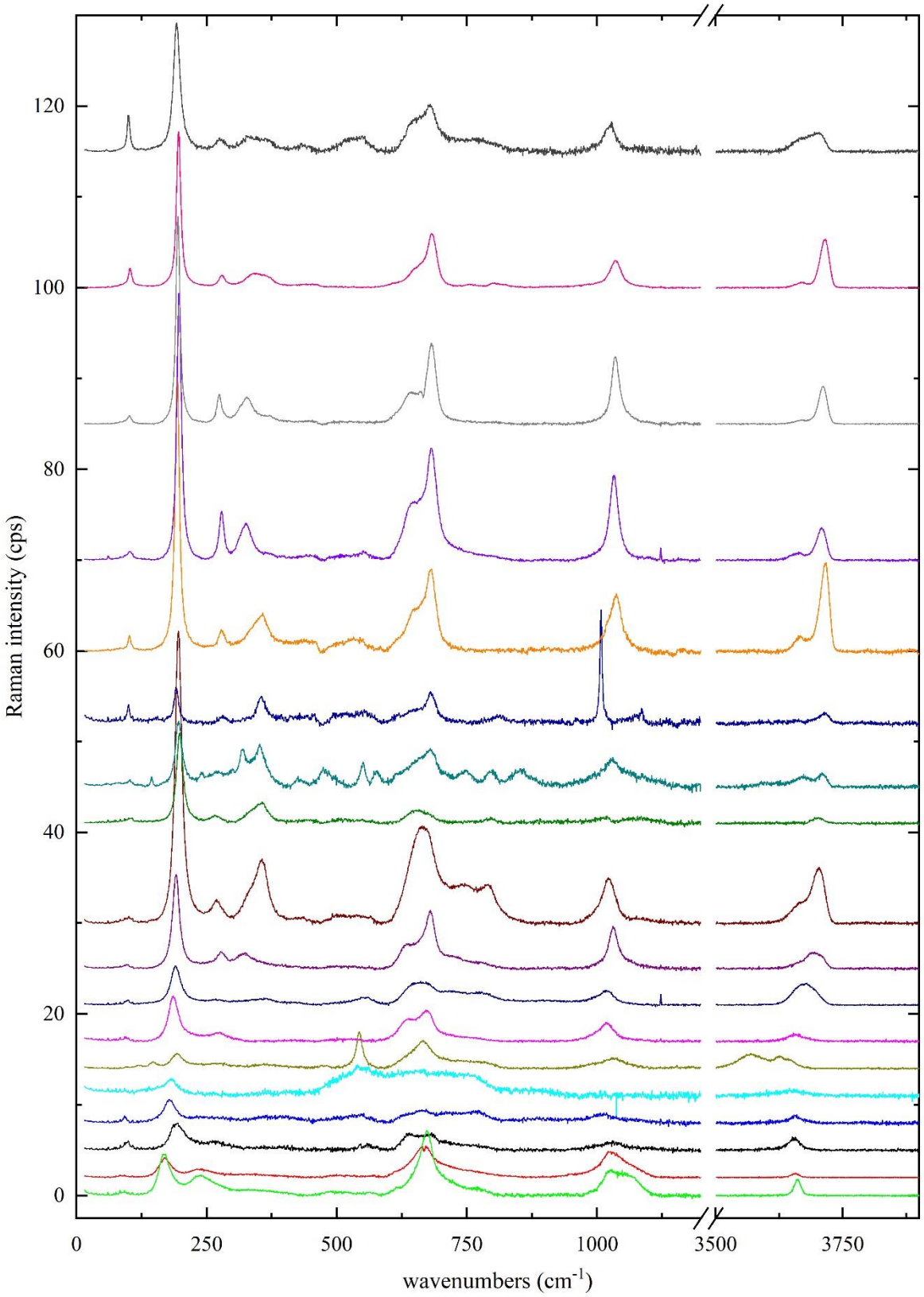

Figure S3: Raman spectra of the studied biotites in vertical parallel-polarized geometry, where ^{M}Mg content increases from bottom to top. Colours are the same as in figure S1 and correspond to equal Mg contents. For better comparison, the spectra are vertically offset.

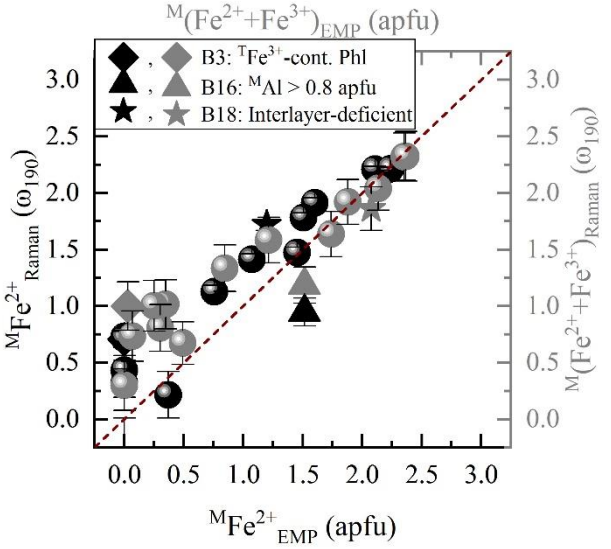

Figure S4: Estimation of $^{M}Fe^{2+}$ and $^{M}(Fe^{2+}+Fe^{3+})$ contents according to MO_6 vibrations: $^{M}Fe^{2+}$ content derived from the Raman spectroscopic analysis ($^{M}Fe^{2+}_{Raman}$) of ω_{190} (black symbols) and $^{M}(Fe^{2+}+Fe^{3+})$ content (grey symbols) vs. that calculated from EMPA [$^{M}(Fe^{2+}+Fe^{3+})_{EMP}$). Deviating points mentioned in the legend are same as in Fig. 5.

Table S1: Average chemical composition (wt. %) and statistical standard deviation (σ) of the studied biotite crystals. FeO, H_2O, and Fe_2O_3 were calculated following the guidelines of the charge balance approach of Li et al. (2020) and via Mössbauer spectroscopy (FeO and Fe_2O_3 of the samples with an asterisk). Abbreviations in the table: T: total; calc.: calculated; b.d.l.: below detection limit; init.: initial; n.d.: not determined.

	B1	**B2**	**B3**	**B4***	**B5**	**B6**	**B7**	**B8**	**B10**
SiO_2	41.9(3)	42.5(1)	35.8(1.1)	36.5(1)	39.5(4)	39.2(3)	40.2(1)	36.6(4)	40.3(8)
TiO_2	1.25(36)	0.27(2)	0.22(2)	3.26(4)	0.75(5)	3.89(5)	0.27(1)	5.53(15)	0.01(3)
Al_2O_3	14.3(1)	12.8(1)	10.9(4)	7.73(8)	14.1(2)	14.3(2)	14.0(1)	16.8(2)	14.6(2)
FeO_T	0.05(5)	1.16(5)	0.98(6)	34.4(2)	5.8(1)	4.99(9)	1.84(7)	6.66(15)	4.20(3)
MnO	b.d.l.	0.001(7)	b.d.l.	0.99(3)	0.04(3)	0.13(2)	b.d.l.	0.008(20)	0.08(1)
MgO	27.8(2)	27.8(1)	23.9(7)	0.41(2)	24.0(2)	21.8(2)	26.9(1)	19.1(5)	24.6(7)
CaO	b.d.l.	b.d.l.	0.01(3)	b.d.l.	0.003(11)	b.d.l.	0.001(5)	0.02(3)	b.d.l.
Na_2O	0.90(4)	0.18(2)	0.16(1)	0.26(2)	0.43(1)	0.18(3)	0.26(1)	0.41(4)	0.18(2)
K_2O	9.39(9)	10.3(1)	8.49(29)	8.37(7)	9.62(10)	9.56(9)	9.91(8)	9.55(26)	10.0(2)
Cr_2O_3	b.d.l.	b.d.l.	b.d.l.	b.d.l.	0.02(2)	0.10(1)	b.d.l.	0.18(1)	b.d.l.
NiO	b.d.l.	b.d.l.	b.d.l.	b.d.l.	0.06(1)	b.d.l.	b.d.l.	0.07(1)	b.d.l.
CuO	b.d.l.	b.d.l.	b.d.l.	b.d.l.	b.d.l.	b.d.l.	b.d.l.	b.d.l.	b.d.l.
ZnO	b.d.l.	b.d.l.	b.d.l.	1.08(2)	b.d.l.	b.d.l.	b.d.l.	b.d.l.	0.001(9)
SrO	b.d.l.	b.d.l.	b.d.l.	b.d.l.	b.d.l.	b.d.l.	0.04(4)	b.d.l.	b.d.l.
BaO	0.20(2)	0.46(2)	0.40(2)	0.04(4)	0.56(2)	0.45(4)	1.35(4)	0.52(3)	b.d.l.
Cl	0.03(4)	0.003(9)	0.38(10)	0.06(1)	0.002(7)	0.35(1)	0.02(2)	0.015(29)	0.01(2)
F	2.43(8)	4.95(9)	4.88(13)	3.77(9)	0.21(3)	0.80(4)	5.37(9)	0.37(16)	0.37(3)
–O=F+Cl	1.03(3)	2.09(4)	2.14(5)	1.60(4)	0.09(1)	0.42(2)	2.26(4)	0.16(7)	0.16(2)
Sum $_{init.}$	97.2(6)	98.4(2)	84.0(2.5)	95.3(3)	94.9(5)	95.3(6)	97.9(2)	95.6(1.4)	94.3(1.2)
FeO $_{calc.}$	n.d.	0.00	0.17	29.52	0.00	0.00	0.13	5.74	0.00
Fe_2O_3 $_{calc.}$	n.d.	1.29	0.88	5.43	6.43	5.54	1.90	1.02	4.67
H_2O $_{calc.}$	2.30	1.79	1.57	1.30	3.49	2.58	1.63	2.46	3.69
Sum $_{calc.}$	99.5(6)	100.3(2)	85.7(2.4)	97.1(1)	99.1(4)	98.5(6)	99.7(1)	98.1(1.3)	98.5(9)

	B12	**B13***	**B14***	**B16**	**B17***	**B18**	**B19***	**B20**	**B21***
SiO_2	34.9(3)	33.7(3)	32.7(7)	34.1(3)	39.4(3)	30.7(2.4)	33.6(4)	35.9(5)	37.0(3)
TiO_2	2.80(5)	3.07(11)	4.60(17)	1.04(3)	2.05(5)	2.14(41)	1.42(3)	5.65(8)	3.58(6)
Al_2O_3	17.9(2)	14.4(2)	14.2(4)	21.6(2)	11.7(1)	16.2(7)	14.9(2)	15.6(3)	6.49(7)
FeO_T	18.6(2)	31.5(3)	27.3(3)	22.0(4)	13.5(2)	30.6(2.1)	25.6(2)	7.68(18)	34.1(3)
MnO	0.3282)	0.52(2)	1.11(4)	0.91(3)	0.29(2)	0.33(4)	0.35(2)	0.02(3)	0.82(31)
MgO	10.2(1)	3.28(5)	5.13(28)	0.81(34)	17.9(2)	5.8(8)	7.07(10)	18.1(3)	0.33(2)
CaO	b.d.l.	0.01(3)	b.d.l.	b.d.l.	0.05(6)	0.12(24)	0.003(14)	0.03(2)	b.d.l.
Na_2O	0.14(1)	0.11(1)	0.29(3)	0.24(1)	0.53(2)	0.02(3)	0.32(4)	0.53(2)	0.15(2)
K_2O	9.13(8)	8.63(15)	8.99(11)	8.74(9)	9.18(14)	6.1(2.8)	9.12(12)	8.8(1.3)	8.16(12)
Cr_2O_3	b.d.l.	b.d.l.	0.001(5)	b.d.l.	b.d.l.	b.d.l.	b.d.l.	0.23(1)	b.d.l.
NiO	b.d.l.	b.d.l.	b.d.l.	b.d.l.	0.001(5)	b.d.l.	b.d.l.	0.02(2)	b.d.l.
CuO	b.d.l.	b.d.l.	b.d.l.	b.d.l.	b.d.l.	b.d.l.	b.d.l.	b.d.l.	b.d.l.
ZnO	0.02(3)	0.07(4)	0.12(2)	0.26(2)	0.11(2)	0.004(17)	0.45(2)	b.d.l.	0.69(2)
SrO	b.d.l.	b.d.l.	b.d.l.	b.d.l.	b.d.l.	b.d.l.	b.d.l.	b.d.l.	b.d.l.
BaO	0.07(4)	0.07(4)	0.15(3)	b.d.l.	0.21(2)	0.007(23)	0.09(4)	0.44(3)	0.13(3)
Cl	0.01(1)	0.08(1)	0.001(7)	0.004(12)	0.07(1)	0.45(16)	0.02(2)	0.002(7)	0.07(1)
F	0.06(7)	0.18(4)	0.82(13)	2.44(8)	3.72(10)	0.23(10)	1.94(8)	0.24(4)	3.73(11)
–O=F+Cl	0.03(3)	0.09(2)	0.35(5)	1.03(4)	1.58(4)	0.20(7)	0.82(3)	0.10(2)	1.59(5)
Sum $_{init.}$	94.2(5)	95.5(5)	95.0(1.2)	91.1(6)	97.1(4)	92.6(2.8)	94.0(7)	93.1(1.6)	93.7(6)
FeO $_{calc.}$	16.48	23.64	21.93	22.03	12.02	17.66	21.40	5.78	30.75
Fe_2O_3 $_{calc.}$	2.41	8.76	6.02	0.00	1.54	14.39	4.70	2.11	3.71
H_2O $_{calc.}$	3.17	2.95	2.29	2.37	1.66	3.06	2.62	2.31	1.22
Sum $_{calc.}$	97.6(4)	99.3(3)	97.9(9)	93.5(2)	98.9(2)	97.1(7)	97.1(5)	95.6(1.4)	95.3(3)

Table S2: Mössbauer parameters determined by the Voigt based hyperfine distribution approach; IS = isomer shift (mm/s), QS = quadrupole splitting (mm/s), HWHM = Lorentzian half width at half maximum (mm/s), σ = Gaussian broadening to the underlying Lorentzian line width (mm/s), and A = relative area fraction.

Sample	χ^2	IS (mm/s)	QS (mm/s)	HWHM (mm/s)	σ (mm/s)	A (%)	Species
B4		1.145(2)	2.175(3)		0.389(4)	85.7(5)	$^{M}Fe^{2+}$
	0.645	0.404(2)	0.867(4)	0.123(8)	0.270(4)	10.1(4)	$^{M}Fe^{3+}$
		0.239(2)	0.236(4)		0.053(3)	4.2(5)	$^{T}Fe^{3+}$
B13*		1.15(2)	1.894(14)	0.15(2)	-	7.4(1.9)	$^{M}Fe^{2+}$
	0.721	1.151(9)	2.416(11)	0.151(6)	-	67.7(1.8)	$^{M}Fe^{2+}$
		0.309(13)	0.947(14)	0.172(5)	-	24.9(1.2)	$^{M}Fe^{3+}$
B14	0.807	1.133(2)	2.241(4)	0.124(6)	0.368(4)	80.2(4)	$^{M}Fe^{2+}$
		0.4188(3)	0.827(5)		0.249(3)	19.8(5)	$^{M}Fe^{3+}$
B17	0.685	1.123(2)	2.367(4)	0.134(5)	0.297(4)	89.1(7)	$^{M}Fe^{2+}$
		0.469(4)	0.788(3)		0.282(4)	10.1(8)	$^{M}Fe^{3+}$
B19	0.673	1.136(3)	2.311(5)	0.113(8)	0.385(4)	83.5(5)	$^{M}Fe^{2+}$
		0.416(3)	0.945(5)		0.272(4)	16.5(7)	$^{M}Fe^{3+}$
B21		1.151(3)	2.204(5)		0.362(5)	90.3(5)	$^{M}Fe^{2+}$
	0.685	0.427(5)	0.711(7)	0.124(5)	0.121(4)	5.0(7)	$^{M}Fe^{3+}$
		0.192(4)	0.556(5)		0.098(5)	4.7(5)	$^{T}Fe^{3+}$

* σ values not applicable for sample B13, due to the high fraction of magnetite (~ 70%) and thus the data were fitted with Lorentzian shaped lines and a full static Hamiltonian behind QS, IS, and internal magnetic field of magnetite. No Gaussian broadening of the lines is applied here.